# A New Geostationary Satellite-Based Snow Cover Recognition Method for FY-4A AGRI

Haiwei Qiao ⬤, Ping Zhang ⬤, Zhen Li ⬤, *Member, IEEE*, and Chang Liu ⬤

*Abstract*—Snow cover is an important component of the cryosphere. Clouds have a large influence on optical remote sensing satellites when recognizing snow cover. Geostationary satellites, due to their high-frequency observations over coverage areas, can effectively compensate for the drawback of snow cover recognition from polar orbit optical satellites under cloud-covered conditions. However, past geostationary satellites have relatively few band settings to produce sensitive factors for snow cover recognition. The FY-4A Advanced Geostationary Radiation Imager (AGRI) satellite has the advantage of high temporal resolution with a wealth of bands, which highlights its potential in reducing the impact of clouds and accurately obtaining snow cover information. Based on the advantages of FY-4A AGRI data and the flow characteristics of clouds, we developed an improved maximum brightness temperature image synthesis algorithm, which can greatly reduce the probability of cloud and snow cover misclassification. Combining the features of FY-4A AGRI data, we reorganized the snow cover recognition factor and developed a new snow cover recognition method. The results show that the proposed method can reduce cloud cover by 57.172% compared with MOD10A1 data. After evaluating the proposed method using meteorological ground observation datasets and MOD10A1 data, we found that the overall accuracy of the proposed method can reach 94.11% and 98.55%, respectively, and the F-score (FS) can reach 73.05% and 85.40%, respectively.

*Index Terms*—China, Fengyun-4A (FY-4A) advanced geostationary radiation imager (AGRI), geostationary satellite, snow cover.

## I. INTRODUCTION

S NOW cover is one of the most important surface characteristics on Earth that influences surface radiation, energy, and hydrological budgets [1]–[3]. Snow cover information has been utilized in operational snowmelt, runoff forecasting, data assimilation, and the calibration or validation of various hydrological models [4]–[6]. Traditional snow cover monitoring work is carried out through meteorological ground observation datasets, but meteorological ground observation datasets have poor spatial characteristics, which are very limited in regard to snow cover recognition [4], [7], [8]. In recent years, with the rapid increase in the number of remote sensing satellite platforms, remote sensing satellite monitoring of snow cover has been widely used [9]. Polar-orbiting satellites have been continuously observing global snow cover for a long time [10]. Synthetic aperture radar (SAR) completely overcomes the influence of clouds in regard to snow cover recognition [11]. In addition, the emergence of new-generation geostationary orbit satellites has made it possible to monitor snow cover on a large scale in real time.

At present, polar-orbiting optical remote sensing satellite data can be used to monitor snow cover effectively. Snow cover exhibits a specific spectral characteristic compared with other natural surfaces and clouds, with high reflectance in the visible band similar to that of clouds, but in the shortwave band (1.6 $\mu$m) it has lower reflectance than clouds [4], [12]. Thus, the SNOMAP algorithm was proposed to distinguish snow from other surface reflectance effectively for Landsat 5 Thematic Mapper data using this rule. Based on this algorithm, MODIS snow cover products MOD10A1 and MYD10A1 of the National Aeronautics and Space Administration have been widely used [2], [13]. Even though Landsat optical remote sensing satellite data have a high spatial resolution [14]–[16], the probability of clouds in satellite transit time is large, which will have a great impact on the snow cover recognition process [17]–[19]. MODIS uses a combination of two satellites to increase the observation frequency of snow cover [20]–[23], but the daily snow area map of MODIS often encounters data gaps, and snow cover recognition is still severely interfered with by clouds [25].

In recent years, for optical polar-orbiting satellite data, many cloud removal methods have been developed using the principle of fusion of multisensor data or spatiotemporal fusion, and good cloud removal effects have been obtained in some typical snow-covered areas [26]–[28]. In addition, a good way to reduce the influence of clouds on snow cover recognition is to increase the frequency of observations [29]–[32]. The geostationary satellite has the characteristics of a wide imaging range and high temporal resolution, which can effectively reduce the amount of clouds in the observation area through the characteristics of clouds varying with time. The Geostationary Operational Environmental satellite (GOES) series has enabled automated snow cover recognition over North America for a long time [7], [33]–[39]. The Meteosat Second Generation (MSG) satellite continues
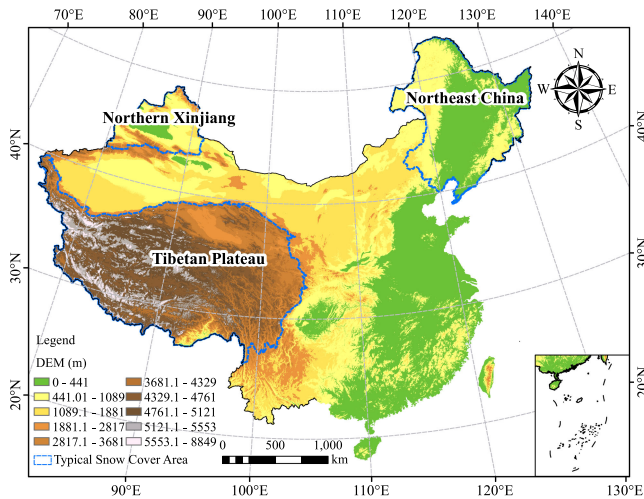
Fig. 1.    Location of the study area. The research area is all China. The blue line surrounds the boundaries of China's three typical snow-covered regions; namely, Northern Xinjiang, Northeast China, and the Tibetan Plateau. The digital elevation model scenes, as the background in the inset below, display the main geomorphological features in these respective areas.

The FY-4A satellite was successfully launched on December 11, 2016, and began to provide data download services on March 12, 2018. The advanced geostationary radiation imager (AGRI) on the FY-4A satellite is a multispectral imager with 14 bands that completes a full disk scan every 15–60 min [55]. In this study, we proposed an improved maximum brightness temperature synthesis algorithm to fuse the daily multitemporal data. Second, we used a new method to recognize snow cover in China. Then, meteorological ground observation datasets, MOD10A1 V6 data, and IMS data were used to evaluate the cloud removal effect and the accuracy of the proposed method. Finally, the reasons that affect the accuracy of snow cover recognition were analyzed.

The rest of this article is organized as follows. Section II mainly introduces the basic situation of the research area and research data. In Section III, the method establishing snow cover recognition for the FY-4A AGRI satellite is introduced. In Section IV, the performance of the snow cover recognition method is evaluated. In Sections V and VI, the uniqueness and shortcomings of the method are discussed and summarized, and the future direction for improvement is briefly described.

## II. STUDY REGION AND DATA

### A. Study Region

China is located in East Asia and the western edge of the Pacific Ocean. It has a land area of $960 \times 10^4$ km$^2$ and a land boundary of more than $2 \times 10^4$ km$^2$ [56]. The terrain is high in the west and low in the east, and the climate is complex and diverse. The snow cover of China is very widespread, with an average snow cover area of more than $900 \times 10^4$ km$^2$ over many years [56]–[58]. The area of stable snow cover reaches $420 \times 10^4$ km$^2$. The three main typical snow cover areas (see Fig. 1) include Tibetan Plateau, Northeast China, and Northern Xinjiang [56]–[59]. Areas with annual average snow cover days greater than 30 days account for 56% of the territory of the country, including two major areas in northeastern and western China. The 20-day contour of average annual snow cover days divides China into two parts: the southeastern and the northwestern, except for the Tarim Basin and Qaidam Basin.

### B. FY-4A AGRI Data

FY-4A is the first satellite in the second-generation geostationary orbit quantitative remote sensing satellite series of China. As a new generation of geostationary orbit meteorological satellites, their functions and performance have achieved leapfrog development [60]. FY-4A carries a variety of observation instruments, including an AGRI, interference atmospheric vertical detector, lightning imager, and space environmental monitoring instrument. Among them, AGRI is one of its main loads. It can achieve precise and flexible two-dimensional pointing through precise dual scanning mirrors and can achieve rapid regional scanning in minutes [60]. Radiation imaging channels increased from 5 found on FY-2G satellites to 14, covering visible light, shortwave infrared, midwave infrared, and longwave infrared. The observation range mainly covers Asia, Oceania, and parts of

to observe the snow cover in the Eurasian region, and after verifying the MSG snow cover product by using meteorological ground observation datasets and MODIS, it was found that the cloud cover had been significantly reduced [40]–[43]. The binarized snow cover recognition algorithm developed based on the FengYun-2 (FY-2) satellite monitors the snow cover in East Asia in real-time [44]. For multispectral remote sensing images, the normalized difference snow index (NDSI) is very effective for snow cover monitoring [45]–[49]. However, in the past, geostationary satellites were limited by technical factors, and most geostationary satellites could not construct factors similar to NDSI for snow cover recognition. Therefore, snow cover recognition has created large uncertainties.

Compared  with optical remote sensing satellites, SAR satellites can penetrate clouds and the atmosphere, and their working hours are not affected by weather or other factors. With the advantages of all-time, all-weather, multipolarization, and multiband imaging, they play an important role in snow cover recognition and greatly compensate for the disadvantages of optical satellites affected by clouds. SIR-C/X-SAR data have been used to study the scattering characteristics of snow, two decision tree snow cover recognition methods have been developed, and a good snow cover recognition effect has been obtained [50]. Radarsat and ERS data have proven to be able to obtain high-precision snow cover recognition [11], [51], and when the threshold is −3 dB, dry and wet snow can be distinguished well [51]. Although SAR satellites have these significant advantages in snow cover recognition, the visual effect of SAR images is lower than that of optical remote sensing satellite images. Therefore, certain obstacles may result in sample selection.

With the launch and operation of new advanced geostationary weather satellites, such as the Himawari-8 and FengYun-4A (FY-4A) satellites, the accuracy of snow cover recognition in China has become increasingly accurate [25], [52]–[54].

TABLE I
MAIN PERFORMANCE OF THE FY-4A AGRI GEOSTATIONARY SATELLITE
RADIATION IMAGER

| Wavelength/μm | Spatial resolution/km | Main uses |
|---|---|---|
| 0.55–0.75 | 0.5 | vegetation, fog, cloud |
| 1.36–1.39 | 2 | cirrus clouds |
| 1.58–1.64 | 2 | low clouds, snow, water clouds |
| 3.5–4.0 | 4 | water and fog |
| 10.3–11.3 | 4 | land surface temperature |
| 11.5–12.5 | 4 | land surface temperature |



Fig. 2. FY-4A AGRI data snow cover recognition new method flowchart. Among them, the blue part is the input and output data, and the green part is the method and data processing process.

Europe, which is basically the same as the observation range of the Himawari-8 geostationary satellite. Table I is a summary of the main performance of the FY-4A AGRI geostationary satellite radiation imager used in this study.

*C. Meteorological Ground Observation Dataset*

Long-term ground observations from November 2018 to January 2020 were collected from meteorological stations over China. Station geographic details include name, ID, latitude, longitude, and altitude, as well as observed snow depth, and these data were available from climate records provided by the National Satellite Meteorological Center [61]. The meteorological ground observation dataset is used to evaluate the accuracy of snow cover recognition results. The principles for selecting the meteorological ground observation dataset are as follows:

1) according to the dataset usage instructions, the outliers (i.e., 32 766 or 32 700) were filtered and eliminated;
2) meteorological stations located in northern Xinjiang, the Tibetan Plateau, and Northeast China were selected; and
3) the data of two snow seasons were selected.

*D. Remote Sensing Data*

The MOD10A1 V6 snow cover product, with a 500 m spatial resolution and HDF format, provides daily binary snow cover data and fractional snow cover data [62]. The MOD10A1 V6 data contain a total of seven datasets. This study uses two datasets, NDSI Snow Cover and NDSI Snow Cover Class, to compose the MOD10A1 V6 snow cover data. Compared with MOD10A1 V5 data, MOD10A1 V6 data use various masks to improve the snow cover recognition algorithm, as well as the accuracy of snow cover recognition.

IMS data are a fusion of 28 types of raw data, including NOAA-AVHRR sensors, GOES, GMS synchronous weather satellites, MTSAT multifunctional satellites, and NIC weekly sea ice analysis products [63], [64]. IMS data provide reliable cloudless snow cover in the Northern Hemisphere. The data have a temporal resolution of 1 day and a spatial resolution of 4 km.

MCD12Q1 land cover type data are used for sample selection when correcting the angular effect of geostationary satellites. The spatial resolution of MCD12Q1 data is 500 m, and the temporal resolution is 1 a. Land cover types are mainly divided into 17 categories, including 11 natural vegetation types, 3 land development, and mosaic types, and 3 nonvegetable land types [65].
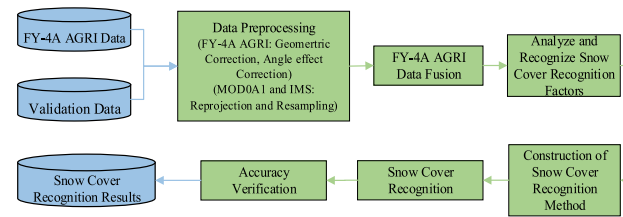
## III. METHOD

In this section, a new method for snow cover recognition based on FY-4A AGRI geostationary satellite data was proposed, as shown in Fig. 2. First, preprocessing was performed on the research data, including geometric correction of FY-4A AGRI data, radiation correction of FY-4A AGRI data, angular effect correction of FY-4A AGRI data, and reprojection and resampling of MOD10A1 data and IMS data. Then, based on the advantages of geostationary satellites with a high temporal resolution, the proposed improved maximum brightness temperature synthesis algorithm was used to reduce the clouds from the image. Through the analysis of the ground reflectance spectrum curve and FY-4A AGRI data characteristics, the appropriate snow cover recognition factor was trained to construct the proposed snow cover recognition method. Finally, the method for evaluating the accuracy of the method was introduced.

*A. Data Preprocessing*

Geometric correction of FY-4A AGRI data: To facilitate the analysis and comparison with other data, FY-4A AGRI data were reprojected and resampled to 0.04° using the official latitude and longitude lookup table.

For the calculation of reflectance and brightness temperature of FY-4A AGRI data, the data used by the proposed method include visible light band reflectance (0.55–0.75 μm), near-infrared band reflectance (1.36–1.39 μm and 1.58–1.64 μm), brightness temperature in two far-infrared bands (10.3–11.3 μm and 11.5–12.5 μm) and mid-infrared band brightness temperature (3.5–4.0 μm). The FY-4A AGRI data contain the lookup table data of the reflectance and brightness temperature corresponding to each band. By correlating the original grey value data with the lookup table, the reflectance and brightness temperature data of the required band can be obtained.

Angle effect correction of FY-4A AGRI data: Geostationary satellites have high temporal resolution and can observe the same feature several times within a day. However, because the imaging time of each scene image is different and the single imaging range is wide, the satellite zenith angle and satellite azimuth angle of pixels have great differences over time, even for the same solar zenith angle, which causes the reflectance of the same feature to change continuously throughout the day [66]. This phenomenon has a significant effect on the visible light band, which greatly affects the threshold value for snow cover recognition. Therefore, the angle effect of the geostationary satellites
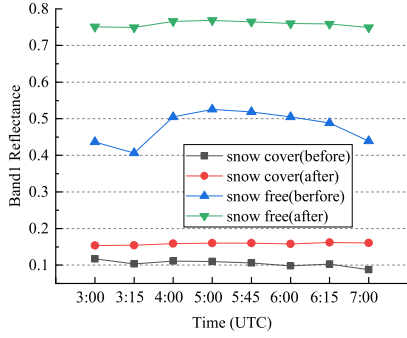
Fig. 3. Comparison of reflectance before and after the angle effect correction in the first band. The four lines show the changes in the reflectance of the snow-covered pixel and the snow-free pixel before and after the angle effect correction during the day, respectively.



Fig. 4. Characteristics of clouds in the thermal infrared band (10.3–11.3 $\mu$m) of FY-4A AGRI data. The boxes of the same color in the figure indicate areas with obvious characteristics. (a) Brightness temperature of 10.3–11.3 $\mu$m. (b) True color synthetic image.

must be corrected. This study used a semiempirical model that combined the advantages of empirical statistical models and physical models [66]. The model is mainly composed of three parts as shown in (1), which contains two kernel functions, two kernel coefficients and a constant. (2) and (3) are kernel functions of $K_{vol}$ and $K_{geo}$, where $\theta_i$ is the solar zenith angle, $\theta_v$ is the satellite observation zenith angle, $\varphi$ is the relative azimuth angle, and g is the phase angle. The angle effect correction method of the semiempirical nuclear drive model proved to be an effective method to solve the angle effect problem of geostationary satellites [9]. Various samples needed in the model were selected with reference to MCD12Q1 data.

$$R(\theta_i, \theta_v, \varphi) = \alpha_0 + \alpha_1 K_{vol}(\theta_i, \theta_v, \varphi) + \alpha_2 K_{geo}(\theta_i, \theta_v, \varphi) \tag{1}$$

$$K_{vol}(\theta_i, \theta_v, \varphi) = \frac{4[(0.5\pi - g) + \cos g + \sin g]}{3\pi(\cos\theta_i + \cos\theta_v)} - \frac{1}{3} \tag{2}$$

$$K_{geo}(\theta_i, \theta_v, \varphi) = \frac{\tan\theta_i \tan\theta_v[(\pi - \varphi)\cos\varphi + \sin\varphi]}{2\pi} - \frac{1}{\pi}$$
$$\left(\tan\theta_i + \tan\theta_v + \sqrt{\tan^2\theta_i + \tan^2\theta_v - 2\tan\theta_i \tan\theta_v \cos\varphi}\right) \tag{3}$$

After correction through the angle effect, we took the FY-4A AGRI first band reflectance data of eight scenes on November 15, 2019 as an example. The reflectance of the snow pixel and the snow-free pixel were selected before and after correction for comparison. It was found that the reflectance variance of the corrected data was smaller than that of the data before correction, as shown in Fig. 3, which reduced the error caused by the angle effect.

For the reprojection and resampling of MOD10A1 data and IMS data, the projection and resolution of MOD10A1 data and IMS data were inconsistent with FY-4A AGRI data. Therefore, the two types of data used for accuracy assessment needed to be reprojected and resampled. This study completed the preprocessing of MOD10A1 data using Google Earth Engine. The spatial resolution of the IMS data was consistent with the FY-4A AGRI data, therefore, only reprojection work was performed.
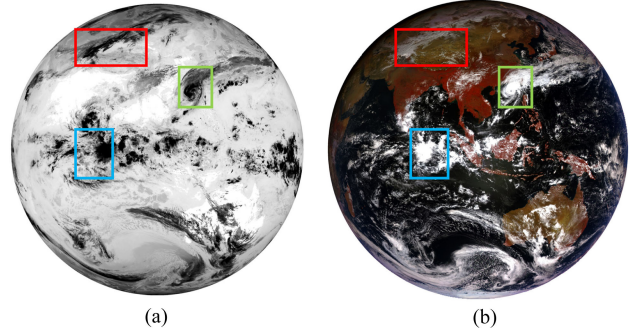
### B. Improved Maximum Brightness Temperature Image Synthesis Algorithm

The greatest advantage of geostationary satellites is their high temporal resolution, which can achieve real-time observations of ground objects. The temporal resolution of FY-4A AGRI data is basically within 60 min, and the data in a day can reach 8–20 scenes. Taking advantage of the high temporal resolution of geostationary satellites, we can reduce the influence of clouds through the characteristics of cloud flow. In past research, the method, which first recognized snow cover and then fused the snow cover recognition results, was affected by the angle effect, and the uncertainty in the selection of the threshold was relatively large. As a result, the overall accuracy of the snow cover recognition results compared with the MOD10A2 data was only 85.25% [67]. Therefore, we fused multitemporal remote sensing images first and then recognized snow cover in this research. According to the spectral reflectance curve of the ground objects, the brightness temperature of the cloud in the far (thermal) infrared band was lower than that of other ground objects, as shown in Fig. 4. In addition, this study used the method of statistical minimum reflectance to improve the maximum brightness temperature image synthesis algorithm, which effectively reduced the cloud cover and controlled the invalid value of the synthesized image.

The traditional algorithm was that in the infrared channel (IR1), the brightness temperature of the cloud was always lower than the brightness temperature characteristics of other ground objects. The highest brightness temperature of the infrared channel was used in the synthesis of multitemporal data, which means that the brightness temperature of each synthesized pixel was the highest value in a day, as shown in the green part of Fig. 5. However, since the thermal infrared sensor can image both day and night, this causes the cloudless value of the night to be fused into the visible light and near-infrared image, resulting in the degradation of the image quality after synthesis. In this study, the night value of the second band was counted and the standard of invalid value control was set. In other words, if the reflectance value of the second band was valid and met the conditions of the original maximum brightness temperature synthesis algorithm,
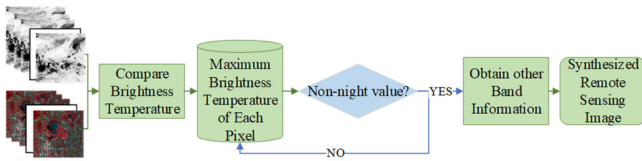
Fig. 5. Flow chart of the maximum brightness temperature influence the synthesis algorithm before and after the improvement. The green part is the original maximum brightness temperature image synthesis algorithm, and the blue part is the improved part.

the reflectance value could be merged into the image. This principle was used to improve the original maximum brightness temperature synthesis algorithm, as shown in the blue part of Fig. 5. Therefore, the total flow in Fig. 5 shows the steps of the improved maximum brightness temperature image synthesis algorithm.

## C. FY-4A AGRI Snow Cover Recognition Method

*1) Analysis of Snow Cover Recognition Factors:* According to the spectral reflectance characteristics of the ground features, the reflectance of snow, vegetation, soil, and other ground features has a large difference in the visible light band of 0.4–0.8 $\mu$m. However, in the visible light band, most characteristics of the cloud reflectance are similar to those of the snow cover, which has a great impact on the recognition of snow cover. In the near-infrared band near 1.36 $\mu$m, there is a large difference in the reflectance of snow and clouds. Therefore, reflectance information in the range of 1.36–1.39 $\mu$m can be used to distinguish between clouds and snow. According to the snow cover recognition algorithm of MSG data, differences of 12.0 and 3.9 $\mu$m brightness temperatures can be used to distinguish between clouds and snow effectively, especially for ice clouds and snow [40]. The maximum brightness temperature image synthesis algorithm shows that the brightness temperature near the 10 $\mu$m band can also be used to distinguish clouds, land, and snow [7].

However, snow and other features cannot be distinguished well based on single-band spectral curve characteristics. To establish a snow recognition method suitable for new geostationary satellite data, we introduced the NDSI proposed by Hall, who also mentioned that the snow cover on vegetation was identified by the normalized differential vegetation index (NDVI) [13]. However, when using FY-4A AGRI data to perform experiments in this article, we found that there was no significant difference in the winter NDVI in Northeast China. Therefore, this research did not use the NDVI. The specific calculation equation of the NDSI is:

$$\text{NDSI} = (\text{R}0.5\,\mu\text{m} - \text{R}1.6\mu\text{m})/(\text{R}0.5\mu\text{m} + \text{R}1.6\mu\text{m}) \tag{4}$$

where $\text{R}_{0.5\mu\text{m}}$ and $\text{R}_{1.6\mu\text{m}}$ represent the reflectance of the band 0.5 $\mu$m and the band 1.6 $\mu$m of FY-4A AGRI data, respectively. Although the NDSI is sensitive to snow, it is also sensitive to some water bodies. Therefore, according to the reflectance spectrum curve of the ground feature, it is known that the reflectance of the water body is low, near the 1.5 $\mu$m band, and
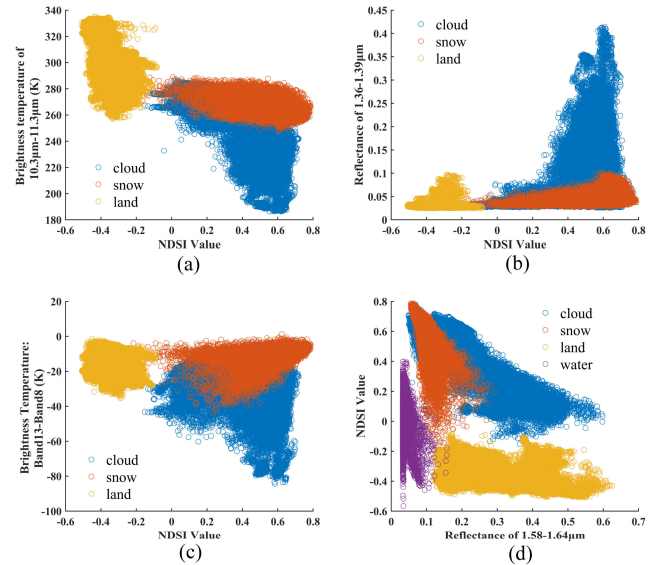


Fig. 6. Sample ground feature separation map: (a) NDSI-brightness temperature of 10.3–11.3 $\mu$m; (b) NDSI-reflectance of 1.36–1.39 $\mu$m; (c) NDSI-the difference between the brightness temperature of Band 13 (11.5–12.5 $\mu$m) and Band 8 (3.5–4.0 $\mu$m); and (d) NDSI-Reflectance of 1.58–1.64 $\mu$m.

this feature can be used to distinguish water from snow. In this way, the NDSI can be effectively used to extract snow.

*2) Training of Snow Cover Recognition Factors for FY-4A AGRI:* This study selected 145 765 samples from the FY-4A AGRI data in January, November, and December 2019. The sample types include snow, clouds, snow-free surfaces, and water. The samples were used to draw the ground object feature map (see Fig. 6). The *x*-axis in Fig. 6(a) is the NDSI value, and the *y*-axis is the brightness temperature in the 10.3–11.3 $\mu$m band. Fig. 6(a) shows that when the value of the NDSI is lower than a certain value, snow-free pixels can be easily separated. When the brightness temperature of the 10.3–11.3 $\mu$m band and NDSI meet certain conditions, partial clouds and snow can be distinguished. The *x*-axis in Fig. 6(b) is the NDSI value, and the *y*-axis is the reflectance of the 1.36–1.39 $\mu$m band. Fig. 6(b) shows that when the NDSI value and the reflectance of the 1.36–1.39 $\mu$m band meet a certain condition at the same time, part of the cloud and snow can also be distinguished. In addition, we also introduced the difference between the brightness temperatures of 11.5–12.5 $\mu$m and 3.5–4.0 $\mu$m to distinguish between clouds and snow, as shown in Fig. 6(c). The *x*-axis in Fig. 6(d) is the NDSI value, and the *y*-axis is the reflectance in the 1.58–1.64 $\mu$m band. Fig. 6(d) shows that snow and water can also be separated when the NDSI value and the reflectivity of the 1.58–1.64 $\mu$m band meet certain conditions at the same time. Therefore, according to the scattered distribution combination of multiple snow cover recognition factors and sample statistics, the snow cover recognition algorithm can be established, and the threshold can be determined.

*3) Construction of the FY-4A AGRI Snow Cover Recognition Method:* According to the basic characteristics of the FY-4A AGRI data and the principles of snow cover recognition, the snow cover recognition factors were selected including the

TABLE II
FY-4A AGRI Snow Cover Recognition Method

| Recognition conditions | Recognition result |
|---|---|
| **First Step** | |
| B12>=296K | no snow |
| NDSI<-0.08 & B12>=257K & B5>=0.11 | no snow |
| NDSI>=0.67 | snow |
| NDSI>=0.45 & B12 >= 268K & -7.405× B5+0.7182 < NDSI | snow |
| CZ>=-12.6K & B12>=268.4K & -7.405× B5+0.7182 < NDSI | snow |
| B12<=248K or B4>0.1007 or CZ <= -40K and -7.405×B5+0.7182 < NDSI | cloud |
| NDSI>-0.08 & -7.4052×B5+0.7182>NDSI & B12>268K | water (no snow) |
| NDSI<=-0.08 & B5<0.11 & B12>268K | water (no snow) |
| **Second Step** | |
| NDSI>=0 & B12<=289K & B4<0.1 & CZ>=-40 & B5<0.11 | snow |
| B12<=268K or B4>=-0.02 | cloud |
| Does not meet any of the above conditions | no snow |

NDSI, the reflectance of the 1.36–1.39 $\mu$m band, the reflectance of the 1.58–1.64 $\mu$m band, the brightness temperature of the 10.3–11.3 $\mu$m band, and the difference between the brightness temperature of the 11.5–12.5 $\mu$m band and the 3.5–4.0 $\mu$m band can effectively recognize snow. Then, we proposed a new snow cover recognition method with two steps, as shown in Table II. The first step was to classify completely determined pixels using two or fewer simple factors, and the remaining unclassified pixels were temporarily divided into complex pixels. The second step was to recombine multiple snow cover recognition factors and then classify the remaining complex pixels. The meaning of each factor in the algorithm is shown in Table II, including that B4 represents the reflectance of Band4 (1.36–1.39 $\mu$m) in the FY-4A AGRI data, B5 represents the reflectance of Band5 (1.58–1.64 $\mu$m) in the FY-4A AGRI data, B12 represents the brightness temperature of Band 12 (10.3–11.3 $\mu$m) in the FY-4A AGRI data, NDSI is the normalized differential snow index, and CZ represents the difference between the brightness temperature of Band 13 (11.5–12.5 $\mu$m) and Band 8 (3.5–4.0 $\mu$m) in the FY-4A AGRI data.

### D. Assessment Metrics

Assessment of snow cover recognition accuracy generally includes consistency checks and nonconsistency checks. A consistency check refers to the degree of similarity between the test result and the assessment value, including the overall accuracy in the absence of clouds (OA) and overall accuracy in the presence of clouds (Qa) [68], [69]. In general, for the MODIS data assessment, only the accuracy assessment under the cloudless condition was considered, as shown in (5). The snow inconsistency test includes an underestimated error (IU) of snow and an overestimated error (IO) of snow. The underestimation error (IU) indicates that the proposed method recognizes snow pixels as snowless pixels, as shown in (6). The overestimation error (IO) indicates that the proposed method recognizes snow-free pixels as snow pixels, as shown in (7). OA considers the probability

under the condition of no snow surface and cannot represent well the consistency of snow cover, and the FS may be more meaningful than OA [70], [71]. The calculation method of FS is shown in (8). Therefore, OA, FS, IU, and IO were chosen as indicators to evaluate the accuracy of the method in this study

$$\text{Overall Accuracy (OA)} = (S1 + S2)/CA \times 100\% \quad (5)$$

$$\text{Underestimation Error (IU)} = D1/CA \times 100\% \quad (6)$$

$$\text{Overestimated Error (IO)} = D2/CA \times 100\% \quad (7)$$

$$\text{F} - \text{Score (FS)} = 2 \times S1/(2\times S1+D1+D2)$$
$$\times 100\% \quad (8)$$

where S1, S2, D1, D2, and CA are pixel numbers. For example, S1 is the number of pixels in which both reference data and method recognition data are snow. S2 is the number of pixels in which both reference data and method recognition data are non-snow. D1 is the reference data recognized as snow pixels, and the method recognition data are non-snow pixels. D2 is the reference data recognized as non-snow pixels, and the method recognition data are snow pixels. CA is the sum of the number of pixels involved in the calculation.

## IV. Results

Meteorological ground observation datasets are usually used for snow cover recognition accuracy assessment. However, meteorological ground observation datasets do not have good spatial characteristics, and this article combined ground observation and remote sensing data to evaluate the proposed method. Through the accuracy analysis of MOD10A1 using data from 223 meteorological stations in China, it was found that the snow cover recognition accuracy of MOD10A1 data in China was as high as 94.3% under cloud-free conditions [69]. The NDSI threshold of the official MOD10A1 V6 version is 40, while it was proven that snow cover recognition is more accurate when the NDSI threshold is 10 in China and the overall accuracy can reach 97.5% [72]. Therefore, the MOD10A1 snow cover products produced by the two thresholds were used for accuracy assessment. One main data source of IMS data is microwave remote sensing data, which can evaluate the accuracy of snow cover recognition after cloud removal without being affected by clouds [73]. However, the overall accuracy of IMS data in stable snow cover areas of China can only reach approximately 88% [73]; therefore, the IMS data are only used to visually compare the accuracy of the snow cover recognition results of the proposed method. Therefore, in this study, first, the MOD10A1 data and IMS data were used to visually compare and analyze the snow cover recognition results of the proposed method. Then, the quantitative accuracy calculation of the snow cover recognition results of the proposed method was carried out using meteorological ground observation datasets and MOD10A1 data. Finally, the MOD10A1 data were used to evaluate the cloud removal effect of the proposed method.

We chose the entire area of China and three typical snow cover areas of China to evaluate the accuracy. The three typical snow cover areas are shown in Fig. 1 as North Xinjiang, Northeast
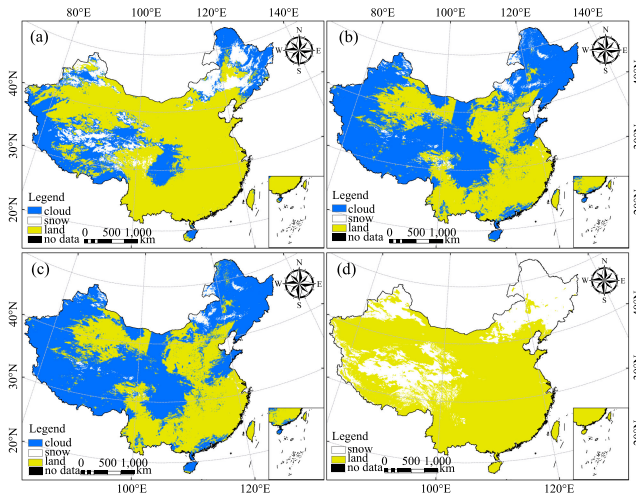
Fig. 7. Comparison of snow cover recognition results in China on 13 December 2019: (a) FY-4A AGRI snow cover recognition results in China on December 13, 2019. (b) MOD10A1(NDSI = 10) snow cover recognition results in China on December 13, 2019. (c) MOD10A1(NDSI = 40) snow cover recognition results in China on December 13, 2019. (d) IMS snow cover recognition results in China on 13 December 2019.
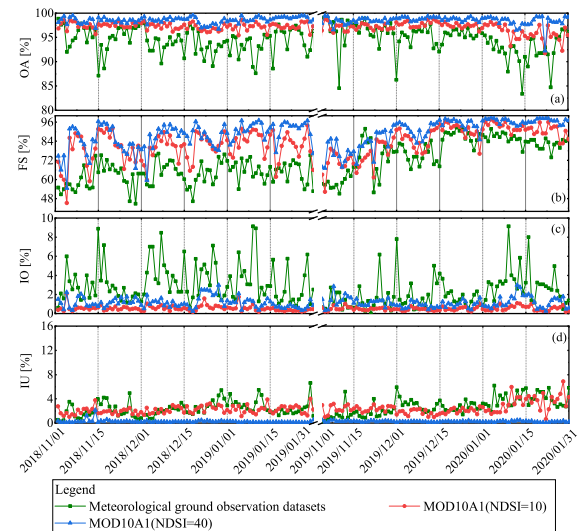


Fig. 8. FY-4A AGRI snow cover recognition results time series analysis. (a) Overall accuracy of China. (b) FS of China. (c) Overestimation error of China. (d) Underestimated error of China.

China, and the Tibetan Plateau. The snow cover in North Xinjiang and Northeast China is mainly stable, while the snow cover in Northeast China is greatly affected by vegetation. The snow cover on the Tibetan Plateau is mainly instantaneous and stable snow cover, and the snow cover is relatively broken, therefore, it is usually difficult to recognize.

### A. Results in China

From Fig. 7, we can compare the snow cover recognition ability and cloud removal effect of the proposed method. Taking the snow cover recognition results on December 13, 2019, as an example, comparing the snow cover recognition results of the FY-4A AGRI [see Fig. 7(a)] and two thresholds of MOD10A1 [see Fig. 7(b) and (c)], it is found that the snow cover recognition results of the FY-4A AGRI can obtain more snow pixels. This is mainly because many clouds were eliminated by using the high temporal resolution of geostationary satellite data. To prevent the multijudgment of snow pixels caused by the misjudgment of clouds and snow, the IMS data [see Fig. 7(d)] that were not affected by clouds are introduced for comparison, and it is found that most snow pixels of the FY-4A AGRI are accurate. It is also obvious from Fig. 7 that the improved maximum brightness temperature synthesis algorithm has a very significant effect on removing clouds.

According to the accuracy assessment method mentioned above, the accuracy of the proposed method was evaluated under cloud-free conditions. First, using meteorological ground observation datasets to evaluate the accuracy of the proposed method, it was found that the average overall accuracy was 94.11%, the average overestimated error was 3.05%, the average underestimation error was 2.84%, and the average FS was 73.05%. Second, the MOD10A1 snow cover product with an NDSI threshold of 10 was used to evaluate the accuracy

of the proposed method. The average overall accuracy was 97.01%, the average overestimated error was 0.68%, the average underestimation error was 2.31%, and the average FS was 81.76%. Finally, using the MOD10A1 snow cover product with an NDSI threshold of 40 to evaluate the accuracy of the proposed method, it was found that the average overall accuracy was 98.55%, the average overestimated error was 1.17%, the average underestimation error was 0.28%, and the average FS was 85.40%. The overall accuracy of the proposed method was relatively high, but the FS value was relatively low, indicating that the proposed method overestimated or underestimated snow pixels when recognizing snow cover. We consider that the main reason for this situation was that, on the one hand, the low spatial resolution of the geostationary orbit satellite data resulted in a large number of mixed pixels being misclassified, and on the other hand, the proposed method may have weak recognition ability in complex snow pixels; for example, snow pixels in mountainous and forested areas.

Fig. 8 shows the time sequence analysis after the accuracy assessment of the snow cover recognition results of the two snow seasons from November 2018 to January 2019 and November 2019 to January 2020 using meteorological ground observation datasets and MOD10A1 data. From the overall accuracy [see Fig. 8(a)], it can be seen that the overall accuracy of snow cover recognition of the FY-4A AGRI can reach 85–100% evaluated by meteorological ground observation datasets and MOD10A1 (both NDSI thresholds). From the FS [see Fig. 8(b)], when the FS was low, it was middle and late November each year, and the FS was only 50–70%. The months with higher FSs were January and December each year, and the FS could reach 70–99%. According to meteorological data, November was the initial stage of snow accumulation, and the snow depth was small, which led to the low accuracy of the FY-4A AGRI snow cover recognition results. From the perspective of misclassification error [see Fig. 8(c) and (d)], when using meteorological ground observation datasets
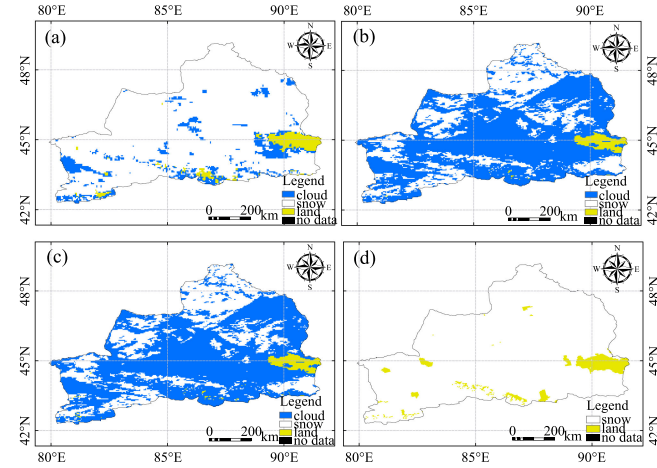
Fig. 9. Comparison of snow cover recognition results in North Xinjiang on January 15, 2019. (a) FY-4A AGRI snow cover recognition results in North Xinjiang on January 15, 2019. (b) MOD10A1(NDSI = 10) snow cover recognition results in North Xinjiang on January 15, 2019. (c) MOD10A1 (NDSI = 40) snow cover recognition results in North Xinjiang on January 15, 2019. (d) IMS snow cover recognition results in North Xinjiang on January 15, 2019.

and MOD10A1 (threshold value of 40) for assessment, the overestimated error and underestimation error were basically the same, while when using MOD10A1 (threshold value of 10) for accuracy assessment, the underestimation error was higher than the overestimated error. This may have been caused by the misjudgment of clouds and snow cover in the proposed method and the difficulty of recognizing snow cover in forest areas. In addition, the scattered snow in mountainous areas was also one of the important reasons that caused the underestimation error to be higher than the overestimation error. For the cloud removal effect, we compared it with the cloud cover of MOD10A1 and found that the improved maximum brightness temperature image synthesis algorithm could reduce the cloud cover by 57.172% on average.

### B. Results in North Xinjiang

First, we chose the northern part of the Xinjiang Autonomous Region (42-50°N, 79-92°E) for the typical research area. Northern Xinjiang contains the Altai Mountains (south) and Tianshan Mountains (north). As an arid region of China, agricultural development relies mainly on snow accumulation and ablation to be sustained in this region [69]. By comparing the results of FY-4A AGRI snow cover recognition with MOD10A1 (two thresholds) and IMS data, the accuracy of the proposed method in northern Xinjiang was evaluated. Fig. 9 shows the snow cover recognition results of the FY-4A AGRI [see Fig. 9(a)], MOD10A1 data (two thresholds) [see Fig. 9(b) and (c)], and IMS data [see Fig. 9(d)] on January 15, 2019. Under cloud-free conditions, the snow cover recognition results of the proposed method in northern Xinjiang were basically the same as the MOD10A1 data on that day. Comparing it with the snow cover recognition results of the IMS data on the day, it was found that the FY-4A AGRI could recognize more snow pixels that were covered by clouds in MOD10A1.

TABLE III
ACCURACY VERIFICATION RESULTS IN NORTH XINJIANG

| Data | OA | IO | IU | FS |
|---|---|---|---|---|
| Meteorological ground observation datasets | 95.10% | 1.36% | 3.54% | 96.98% |
| MOD10A1(NDSI=10) | 96.65% | 0.49% | 2.86% | 94.95% |
| MOD10A1(NDSI=40) | 97.56% | 1.69% | 0.75% | 96.21% |

Table III shows the overall accuracy, overestimated error, underestimation error, and FS of the proposed method using meteorological ground observation datasets and MOD10A1 V6 data (two thresholds). The assessment results are the average value of all experimental data. From Table III, both the overall accuracy and the FS in the North Xinjiang region could be maintained above 91.50%, and there was no significant difference between the underestimation error and overestimated error in this region. Therefore, the proposed method in the North Xinjiang region had a higher snow cover recognition accuracy. In addition, compared with MOD10A1 data, the average cloud removal ratio of FY-4A AGRI data after fusion was as high as 68.63%. In general, the accuracy of the FY-4A AGRI snow cover recognition results in North Xinjiang was relatively high, and the spatial distribution of accuracy was closely related to the terrain. In comparison, the overall accuracy and FS in the southern region with higher terrain complexity were lower than those in the northern region. At the same time, the complexity of land cover also had a negative impact on accuracy, especially in areas covered by vegetation, where the accuracy of snow recognition was slightly lower than in other areas. From the perspective of error analysis, it was found that the underestimation error was higher than the overestimation error because the lack of spatial resolution led to difficulty in recognizing snow cover in mountainous areas.

### C. Results in Northeast China

Northeast China (38-54 °N, 115-136 °E) has a variety of climate types, spanning warm, middle, and cold temperate zones. There are abundant forest resources in mountain areas, and there is much snowfall in winter. It is one of the three stable snow regions in China, with an average snow depth above 5 cm. The snow-covered surface in this area is mostly vegetation; therefore, there is a great challenge in recognition. Fig. 10 shows the snow cover recognition results of the FY-4A AGRI [see Fig. 10(a)], MOD10A1 (two thresholds) [see Fig. 10(b) and (c)], and IMS data [see Fig. 10(d)] on January 15, 2020. Through qualitative comparison, the snow cover recognition results of the proposed method were basically consistent with MOD10A1 data and IMS data.

Table IV shows the overall accuracy, overestimated error, underestimation error, and FS of the proposed method using meteorological ground observation datasets and MOD10A1 V6 data (two thresholds) in Northeast China. The assessment data are the average value of all experimental data. From Table IV, using meteorological ground observation datasets for assessment, it was found that the overall accuracy and FS reached 87.97% and
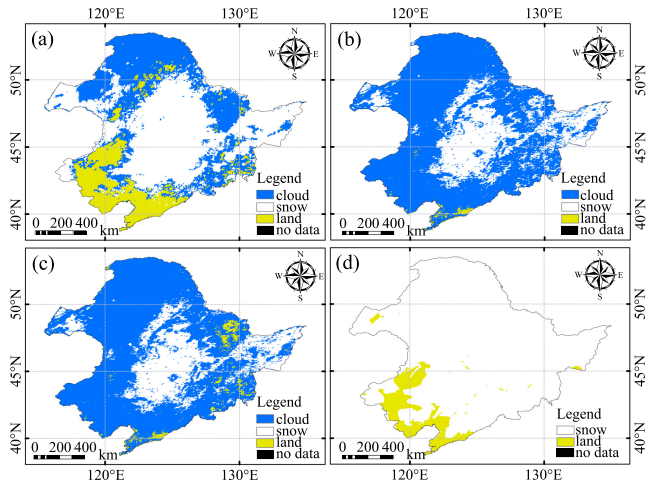
Fig. 10. Comparison of snow cover recognition results in Northeast China on January 15, 2020. (a) FY-4A AGRI snow cover recognition results in Northeast China on January 15, 2020. (b) MOD10A1 (NDSI = 10) snow cover recognition results in Northeast China on January 15, 2020. (c) MOD10A1 (NDSI = 40) snow cover recognition results in Northeast China on January 15, 2020. (d) IMS snow cover recognition result in Northeast China on January 15, 2020.

TABLE IV
ACCURACY VERIFICATION RESULTS IN NORTHEAST CHINA

| Data | OA | IO | IU | FS |
|---|---|---|---|---|
| Meteorological ground observation datasets | 87.97% | 2.97% | 9.06% | 78.46% |
| MOD10A1(NDSI=10) | 96.63% | 0.66% | 2.71% | 81.35% |
| MOD10A1(NDSI=40) | 99.19% | 0.52% | 0.29% | 93.20% |

78.46%, respectively. The main reason for this was that the forest area affects the accuracy of the proposed method for snow cover recognition. Compared with the MOD10A1 data, the overall accuracy and FS of the FY-4A AGRI snow cover recognition results in the Northeast China region were as high as 99.19% and 93.20%, respectively. When the MOD10A1 snow cover product generates snow coverage in the forest area, a more complicated decision tree snow recognition method is adopted, and the spatial resolution of the MOD10A1 data is much higher than that of the FY-4A AGRI data. Therefore, the proposed method has a certain accuracy and simplicity. In terms of errors, there is no significant difference between the overestimation error and the underestimation error using MOD10A1 data for accuracy assessment. The underestimation error of using meteorological ground observations for accuracy assessment is greater than the overestimation error. The underestimation of snow pixels is mainly related to the terrain and underlying surface of the snow cover. The accuracy of snow cover recognition in northeastern China decreases with increasing altitude, mainly because the terrain becomes more complicated with increasing altitude. In particular, forest-covered areas with lower snow cover recognition accuracy have higher elevations and more rugged terrain, which leads to a serious underestimation of snow cover. Another reason may be that Northeast China is located in a higher latitude area. Therefore, when the angle effect is corrected for a large range, the fitted coefficients may not fit Northeast China
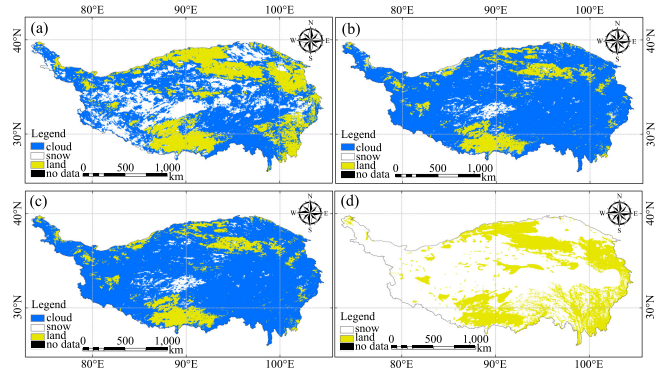


Fig. 11. Comparison of snow cover recognition results on the Tibetan Plateau on January 20, 2020. (a) FY-4A AGRI snow cover recognition results on the Tibetan Plateau on January 20, 2020. (b) MOD10A1 (NDSI = 10) snow cover recognition results on the Tibetan Plateau on January 15, 2020. (c) MOD10A1 (NDSI = 40) snow cover recognition results on the Tibetan Plateau on January 20, 2020. (d) IMS snow cover recognition results on the Tibetan Plateau on January 20, 2020.

TABLE V
ACCURACY VERIFICATION RESULTS IN TIBETAN PLATEAU

| Data | OA | IO | IU | FS |
|---|---|---|---|---|
| Meteorological ground observation datasets | 92.70% | 2.85% | 4.45% | 73.11% |
| MOD10A1(NDSI=10) | 94.50% | 1.09% | 4.41% | 71.26% |
| MOD10A1(NDSI=40) | 96.71% | 2.74% | 0.55% | 75.73% |

well, which affects the normalization of the reflectance. Finally, compared with the MOD10A1 data, the proposed method could reduce the cloud cover by 54.28% on average in this area.

### D. Results in Tibetan Plateau

The Tibetan Plateau is called the roof of the world. Its average elevation is greater than 4000 m, making it the highest plateau in the world. The snow distribution on the Tibetan Plateau has large spatial heterogeneity. Stable snow is mainly distributed in high mountain areas. The snow distribution in mountain areas is dispersive, therefore, it is difficult to recognize snow cover [74]–[76]. Fig. 11 shows the snow cover recognition results of the FY-4A AGRI [see Fig. 11(a)], MOD10A1 (two thresholds) [see Fig. 11(b) and (c)], and IMS data [see Fig. 11(d)] on January 20, 2020. The snow cover recognition results of the proposed method were basically consistent with the recognition range of MOD10A1 data and IMS data. However, there were some misjudgments in the snow pixels in mountainous areas. It can be clearly seen from the figure that despite the cloud removal process, there were still more clouds in the results of the proposed method, which was mainly determined by the weather in the plateau area. At the same time, it is found from the figure that the performance of the proposed method was reduced when recognizing snow cover in mountainous areas, which was mainly related to the spatial resolution of the data and the ability of the method to recognize mixed pixels.

Table V shows the overall accuracy, overestimated error, underestimation error, and FS of the proposed method using

meteorological ground observation datasets and MOD10A1 V6 data (two thresholds) on the Tibetan Plateau. The assessment data are the average value of all experimental data. From Table V, using meteorological ground observation datasets for assessment, it was found that the overall accuracy and FS could only reach 92.70% and 73.11%, and compared with the MOD10A1 data, the overall accuracy and FS of FY-4A AGRI snow cover recognition results on the Tibetan Plateau were 96.71% and 75.73%, respectively, indicating that the snow cover recognition accuracy on the Tibetan Plateau was low. One of the reasons for this phenomenon may have been that the snow cover on the Tibetan Plateau was relatively scattered [74], [75], and the low spatial resolution of the FY-4A AGRI had a problem with mixed pixels. Therefore, it misjudged the snow cover on the Tibetan Plateau. In addition, the main land cover types on the Tibetan Plateau included grassland, bare land, and forest, while the land cover types in areas with lower FSs were mostly sparse forest areas, indicating that the snow cover recognition accuracy on the Tibetan Plateau was related to the underlying surface. It is worth noting that the complexity of the terrain also had a certain impact on the accuracy of snow cover recognition on the Tibetan Plateau. The areas with low snow cover recognition accuracy were mostly in the southeast, where the terrain is more complicated. In terms of the effect of cloud removal, the cloud removal rate on the Tibetan Plateau reached 59.46% compared with MOD10A1.

## V. Discussion

Widespread and persistent cloud cover in time and space has a great impact on the recognition of snow cover by optical satellites, and it is difficult to obtain snow cover information under clouds and to clearly distinguish between clouds and snow cover. Polar-orbiting satellites have accomplished the accurate recognition of snow cover and clouds with their advantages of high spatial resolution and high spectral resolution. However, polar-orbiting satellites are usually limited by temporal resolution and cannot monitor large-scale snow cover changes in real time. Therefore, the daily snow cover recognition results obtained from the optical sensor usually have gaps. In the past, geostationary orbit satellites were affected by the spectral resolution and could not generate some factors that were sensitive to snow cover. In the current study, we took advantage of the high temporal resolution of the new generation geostationary satellite FY-4A AGRI to improve the maximum brightness temperature image synthesis algorithm and proposed a new method for snow cover recognition in China. Our results show that the improved maximum brightness temperature image synthesis algorithm and the proposed method can reduce clouds in images and accurately recognize daily snow cover. The importance of this study is not only that we improved the maximum brightness temperature image synthesis algorithm to reduce cloud cover and invalid values but also that the proposed method can provide accurate snow cover information in a concise way.

In terms of geostationary satellite image synthesis technology, Yang *et al.* [4] proposed a maximum brightness temperature
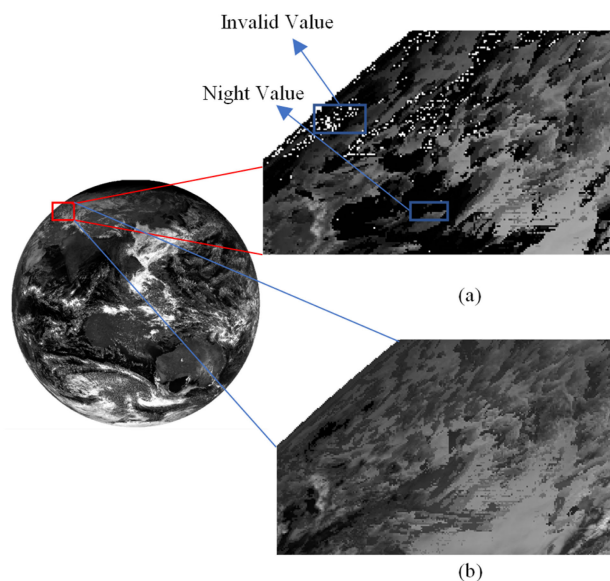


Fig. 12. Comparison figure of the maximum brightness temperature image synthesis algorithm before and after improvement. (a) The fusion figure of the original algorithm. (b) The fusion figure of the improved algorithm.

synthesis algorithm to synthesize MTSAT images to reduce clouds, but the algorithm did not take into account the imaging differences between thermal infrared sensors and visible light near-infrared sensors. Therefore, more night values and invalid values were introduced, and now it seems that the temporal resolution of MTSAT satellites no longer has a major advantage. Based on considering the imaging differences from different types of sensors, we combined the advantages of the high temporal resolution of the new generation geostationary satellite FY-4A AGRI to improve the maximum brightness temperature synthesis algorithm of Yang, reducing the night value and clouds of the synthesized image. Compared with MOD10A1 data, the average cloud removal rate of the improved maximum brightness temperature image synthesis algorithm is 5.27% higher than that of the fusion algorithm proposed by Yang *et al.* [4] and reaches 57.172% in China. In addition, the proportion of cloud removal in the three typical snow cover areas reaches approximately 59.33%. It should be noted that although the efficiency of cloud removal is only increased by 5.27%, the original algorithm incorporates more useless invalid values and night values for cloud removal. Fig. 12 is a comparison diagram of the two algorithms after image fusion. It can be clearly seen that the results of the original algorithm fusion contain a large number of night values and invalid values, and the results of our improved method have alleviated these phenomena.

Romanov and Wildt proposed snow cover recognition algorithms for past geostationary satellites GOES-13 and MSG-2 [1], [3], [7], [34], [35]. However, past geostationary satellites had relatively few band settings, which could not even generate the NDSI. Most indices that are sensitive to snow cover were replaced by the SI index, and the snow cover recognition effect of SI is far inferior to that of NDSI. The FY-4A AGRI sensor

has 14 wavebands, and its wavelength range includes visible light to far-infrared, which can effectively solve this problem. We also studied the results of the past snow cover recognition method for the new generation geostationary orbit satellites. For example, Han [77] proposed a new generation of geostationary satellite decision tree snow cover recognition models based on FY-4A AGRI satellite data from China and Hammria-8 satellite data from Japan. This model reduced the false alarm rate of clouds and snow, but the snow cover recognition factors of this model are very complex and difficult to implement. In addition, Wang *et al.* recognized the snow cover on the Tibetan Plateau based on the Himawari-8 satellite data of Japan, and the snow cover recognition method proposed in this study is limited by the angle effect and is only applicable to the Tibetan Plateau. Although our proposed method only uses some relatively simple snow cover recognition factors, it can be evaluated to obtain high accuracy in the main snow-covered areas of China.

In addition, forest cover is one of the key factors that affect the performance of the optical satellite snow cover recognition algorithm. Muhuri *et al.* [78] used Landsat 7/8 satellite data and Sentinel-2 satellite data to evaluate the performance of SCA and FSC snow cover recognition. The detection performance of these two algorithms is seriously affected by dense tree canopies and low-light forest areas [78]. Similarly, this problem also arises when using geostationary satellite data to recognize snow cover in forest areas. To address this issue, other factors are usually used to recognize snow cover in these areas. For example, Wang *et al.* [79] used the NDFSI to recognize snow cover in forest areas with good results. Hall *et al.* [13] used the NDVI to change the NDSI threshold of snow cover in forest areas. This method is widely used in the snow recognition process of MODIS satellites and Landsat series satellites. However, we found through experiments that these auxiliary recognition factors are not suitable for FY-4A AGRI data. At the same time, we found that the SNOWMAP algorithm and the method proposed by Romanov for GOES-13, which performs better for snow cover recognition in past satellite data, are not fully applicable to FY-4A AGRI data. The main reason for the failure of these mainstream snow cover recognition methods may be the high temporal resolution of geostationary satellites and the excessively wide imaging range. This leads to poor reflectance normalization results so that the threshold setting cannot fully satisfy all areas, especially in a wide range. Although the accuracy of the proposed method is lower when recognizing snow cover in forest areas, it can still accurately recognize snow cover in forest areas without these auxiliary recognition factors. In past research, the accuracy assessment of MOD10A1 data using meteorological ground observation datasets showed that the average overall accuracy and FS of MOD10A1 data in Northeast China during the snow season were only 91.70% and 81.30%, respectively [69]. After verifying the accuracy of the snow cover recognition results of the proposed method using meteorological ground observation datasets, we found that the overall accuracy and FS in Northeast China can also reach 87.97% and 78.46%, which are equivalent to the snow cover recognition accuracy of MOD10A1 data.

The proposed method also has some limitations and deficiencies, which affect the accuracy of snow cover recognition. First, unlike North Xinjiang and Northeast China, the Tibetan Plateau has more snow-free surface pixels, which causes the overall accuracy of the area to be too high. This is because the misjudgment of snow cover is mainly caused by the difficulty of distinguishing between clouds and snow and the difficulty of recognizing snow cover in forest areas. The recognition of snow-free pixels is more accurate, and a large number of snow-free pixels causes the overall accuracy to be overestimated when evaluating snow cover consistency. Therefore, after calculating the FS, these snow-free pixels are discarded, and the snow cover recognition accuracy of the Tibetan Plateau decreases. By analyzing the misclassification error of snow cover recognition on the Tibetan Plateau, it is found that the main cause of the error is the underestimation of the snow pixels, and most missing snow pixels are scattered snow in the mountains. We consider that the reason for this problem is that, on the one hand, the low spatial resolution of FY-4A AGRI data results in a large number of mixed pixels. Therefore, a simple threshold cannot effectively recognize the snow of mixed pixels. On the other hand, the snow cover recognition accuracy of geostationary satellites is affected by the angle effect. When angle effect correction is performed in China, it can only satisfy the best angle effect correction result for the entire area rather than the local area. In addition, the surface types on the Tibetan Plateau are complex, and the accuracy of snow cover recognition is inseparable from the angle effect, which also leads to the low accuracy of snow cover recognition on the Tibetan Plateau. Second, errors in the cloud screening process also affect the accuracy of snow cover recognition. When using the improved algorithm for image fusion, we still only use the features of one band to remove the clouds, which may cause some snow pixels to be misjudged as cloud pixels and are, thus, removed. In addition, in forest areas, compared with snow cover products produced by polar-orbiting satellite MODIS, the overall accuracy of snow cover recognized by FY-4A AGRI data is approximately 4% lower, and the FS is approximately 3% lower. The reason for this phenomenon is that there is uncertainty in the normalization of the reflectance of geostationary satellites, especially when the study area is large and far away from the imaging center, and such uncertainty will greatly increase. Specifically, when trying to add factors such as the NDFSI and NDVI to assist snow cover recognition in the process of snow cover recognition, the FY-4A AGRI data did not show very sensitive changes to the forest area. On the other hand, compared with polar-orbiting satellites, the spatial resolution of geostationary orbiting satellites is still relatively low, which also affects the recognition of snow cover under the canopy. Finally, the poor data quality or sample quality in some areas can lead to some uncertainty in the proposed method. During the accuracy assessment with MOD10A1, we found that there are approximately 7% anomalies in the experimental data, that is, the overall accuracy is less than 90%. The abovementioned problems are expected to be solved through the continuous development of geostationary satellite sensors and the continuous updating of image processing technology. In addition, it should be noted that although deep learning methods can accurately distinguish snow

pixels, attention should also be given to combining deep learning methods with snow physical mechanisms to obtain more reliable snow cover recognition results.

## VI. Conclusion

The main study conclusions are as follows:

1) The improved maximum brightness temperature image synthesis algorithm reduces the invalid value of the synthesized image, and the cloud removal ratio reaches 57.172%. At the same time, the overall accuracy and FS of the proposed snow cover recognition method in China are as high as 94.11% and 73.05%, respectively.

2) After verifying the accuracy with the two cross-assessment datasets, it is found that the snow cover recognition results of the proposed method are highly consistent with the MOD10A1 data, and the overall accuracy and FS are 98.55% and 85.40%, respectively. Combined with the snow cover recognition results of IMS data, it is found that FY-4A AGRI can increase the probability of observing snow pixels under clouds.

3) Affected by many factors, the ability of the FY-4A AGRI snow cover recognition in the three typical snow areas is different. The proposed method can obtain better accuracy in North Xinjiang and Northeast China than that in the Tibetan Plateau.

In summary, the image fusion method and snow cover recognition method proposed in this study can significantly reduce cloud cover and accurately obtain the daily snow cover in China. Therefore, this study is of great significance when acquiring snow cover information.

## Acknowledgment

## References

[1] P. Romanov, G. Gutman, and I. Csiszar, "Automated monitoring of snow cover over North America with multispectral satellite data," *J. Appl. Meteorol.*, vol. 39, no. 11, pp. 1866–1880, Nov. 2000.

[2] Y. Gao, H. Xie, N. Lu, T. Yao, and T. Liang, "Toward advanced daily cloud-free snow cover and snow water equivalent products from Terra–Aqua MODIS and Aqua AMSR-E measurements," *J. Hydrol.*, vol. 385, no. 1–4, pp. 23–35, Jan. 2010.

[3] P. Romanov, D. Tarpley, G. Gutman, and T. Carroll, "Mapping and monitoring of the snow cover fraction over North America," *J. Geophys. Res. Atmos.*, vol. 108, no. D16, pp. 8619–8634, Aug. 2003.

[4] J. Yang, L. Jiang, J. Shi, S. Wu, R. Sun, and H. Yang, "Monitoring snow cover using Chinese meteorological satellite data over China," *Remote Sens. Environ.*, vol. 143, pp. 192–203, Mar. 2014.

[5] T. Barnett, J. Adam, and D. Lettenmaier, "Potential impacts of a warming climate on water availability in snow-dominated regions," *Nature*, vol. 438, no. 7066, pp. 303–309, Nov. 2005.

[6] A. Tait, D. Hall, J. Foster, and R. Armstrong, "Utilizing multiple datasets for snow-cover mapping," *Remote Sens. Environ.*, vol. 72, no. 1, pp. 111–126, Apr. 2000.

[7] P. Romanov and D. Tarpley, "Enhanced algorithm for estimating snow depth from geostationary satellites," *Remote Sens. Environ.*, vol. 108, no. 1, pp. 97–110, May 2007.

[8] G. Wirth, M. Schroedter-Homscheidt, M. Zehner, and G. Becker, "Satellite-based snow identification and its impact on monitoring photovoltaic systems," *Sol. Energy*, vol. 84, no. 2, pp. 215–226, Feb. 2010.

[9] J. Yang, L. Jiang, F. Wu, and R. Sun, "Monitoring snow cover over China with MTSAT-2 geostationary satellite," *J. Remote Sens.*, vol. 17, no. 5, pp. 1264–1280, Mar. 2013.

[10] D. K. Hall, R. E. J. Kelly, G. A. Riggs, A. T. C. Chang, and J. L. Foster, "Assessment of the relative accuracy of hemispheric-scale snow-cover maps," *Ann. Glaciol. Ser.*, vol. 34, pp. 24–30, Sep. 2002.

[11] A. Muhuri, S. Manickam, A. Bhattacharya, and Snehmani, "Snow cover mapping using polarization fraction variation with temporal RADARSAT-2 C-Band full-polarimetric SAR data over the Indian Himalayas," *IEEE J. Sel. Topics Appl. Earth Observ. Remote Sens.*, vol. 11, no. 7, pp. 2192–2209, Jul. 2018.

[12] J. Dozier, "Spectral signature of Alpine snow cover from the Landsat thematic mapper," *Remote Sens. Environ.*, vol. 28, pp. 127–140, Apr.–Jun. 1989.

[13] D. Hall, G. Riggs, and V. Salomonson, "Development of methods for mapping global snow cover using moderate resolution imaging spectroradiometer data," *Remote Sens. Environ.*, vol. 54, no. 2, pp. 127–140, Nov. 1995.

[14] C. Donmez, S. Berberoglu, S. Y. Cicekli, A. Cilek, and A. N. Arslan, "Mapping snow cover using landsat data: Toward a fine-resolution water-resistant snow index," *Meteorol. Atmos. Phys.*, vol. 133, no. 2, pp. 281–294, Apr. 2021.

[15] M. Girona-Mata, E. Miles, S. Ragettli, and F. Pellicciotti, "High-resolution snowline delineation from Landsat imagery to infer snow cover controls in a Himalayan catchment," *Water Resour. Res.*, vol. 55, no. 8, pp. 6754–6772, Aug. 2019.

[16] Z. Mityok, D. Bolton, N. Coops, E. Berman, and S. Senger, "Snow cover mapped daily at 30 meters resolution using a fusion of multi-temporal MODIS NDSI data and Landsat surface reflectance," *Can. J. Remote Sens.*, vol. 44, no. 5, pp. 413–434, Oct. 2018.

[17] S. A. Margulis, Y. F. Liu, and E. Baldo, "A joint Landsat- and MODIS-based reanalysis approach for midlatitude montane seasonal snow characterization," *Front. Earth Sci.*, vol. 7, pp. 272–295, Oct. 2019.

[18] T. Stillinger, D. Roberts, N. Collar, and J. Dozier, "Cloud masking for Landsat 8 and MODIS Terra over snow-covered terrain: Error analysis and spectral similarity between snow and cloud," *Water Resour. Res.*, vol. 55, no. 7, pp. 6169–6184, Jul. 2019.

[19] P. Rastner, R. Prinz, C. Notarnicola, L. Nicholson, and F. Paul, "On the automated mapping of snow cover on glaciers and calculation of snow line altitudes from multi-temporal landsat data," *Remote Sens.*, vol. 11, no. 12, Jun. 2019, Art. no. 1410.

[20] P. Aghelpour, Y. Guan, H. Bahrami-Pichaghchi, B. Mohammadi, O. Kisi, and D. Zhang, "Using the MODIS sensor for snow cover modeling and the assessment of drought effects on snow cover in a mountainous area," *Remote Sens.*, vol. 12, no. 20, Oct. 2020, Art. no. 3437.

[21] S. Hao, L. Jiang, J. Shi, G. Wang, and X. Liu, "Assessment of MODIS-based fractional snow cover products over the Tibetan Plateau," *IEEE J. Sel. Topics Appl. Earth Observ. Remote Sens.*, vol. 12, no. 2, pp. 533–548, Feb. 2019.

[22] G. Riggs and D. Hall, "Continuity of MODIS and VIIRS snow cover extent data products for development of an Earth science data record," *Remote Sens.*, vol. 12, no. 22, Nov. 2020, Art. no. 3781.

[23] H. Vickers, S. Karlsen, and E. Malnes, "A 20-Year MODIS-based snow cover dataset for Svalbard and its link to phenological timing and sea ice variability," *Remote Sens.*, vol. 12, no. 7, Apr. 2020, Art. no. 1123.

[24] H. Tran, P. Nguyen, M. Ombadi, K. Hsu, S. Sorooshian, and X. Qing, "A cloud-free MODIS snow cover dataset for the contiguous United States from 2000 to 2017," *Sci. Data*, vol. 6, Jan. 2019, Art. no. 180300.

[25] G. Wang, L. Jiang, J. Shi, X. Liu, J. Yang, and H. Cui, "Snow-covered area retrieval from Himawari-8 AHI imagery of the Tibetan Plateau," *Remote Sens.*, vol. 11, no. 20, Oct. 2019, Art. no. 2391.

[26] X. Li, Y. Jing, H. Shen, and L. Zhang, "The recent developments in cloud removal approaches of MODIS snow cover product," *Hydrol. Earth Syst. Sci.*, vol. 23, no. 5, pp. 2401–2416, May 2019.

[27] J. Yu, G. Zhang, T. Yao, H. Xie, H. Zhang, and C. Ke, "Developing daily cloud-free snow composite products from MODIS Terra–Aqua and IMS for the Tibetan Plateau," *IEEE Trans. Geosci. Remote Sens.*, vol. 54, no. 4, pp. 2171–2180, Nov. 2016.

[28] Y. Jing, H. Shen, X. Li, and X. Guan, "A two-stage fusion framework to generate a Spatio–temporally continuous MODIS NDSI product over the Tibetan Plateau," *Remote Sens.*, vol. 11, no. 19, Sep. 2019, Art. no. 2261.

[29] T. Miura and S. Nagai, "Landslide detection with Himawari-8 geostationary satellite data: A case study of a torrential rain event in Kyushu, Japan," *Remote Sens.*, vol. 12, no. 11, Jun. 2020, Art. no. 1734.

[30] D. Martinez-de-Rioja, E. Martinez-de-Rioja, J. Encinar, Y. Rodriguez-Vaqueiro, and A. Pino, "Preliminary simulations of flat and parabolic reflectarray antennas to generate a multi-spot coverage from a geostationary satellite," *IET Microw. Antennas Propag.*, vol. 14, no. 14, pp. 1742–1748, Nov. 2020.

[31] Q. Coopman, C. Hoose, and M. Stengel, "Analysis of the thermodynamic phase transition of tracked convective clouds based on geostationary satellite observations," *J. Geophys. Res. Atmos.*, vol. 125, no. 11, Jun. 2020, Art. no. e2019JD032146.

[32] T. Butash, P. Garland, and B. Evans, "Non-geostationary satellite orbit communications satellite constellations history," *Int. J. Satell. Comm. Network.*, vol. 39, no. 1, pp. 1–5, Jan. 2021.

[33] A. Simic, R. Fernandes, R. Brown, P. Romanov, and W. Park, "Validation of VEGETATION, MODIS, and GOES plus SSM/I snow-cover products over Canada based on surface snow depth observations," *Hydrol. Process*, vol. 18, no. 6, pp. 1089–1104, Apr. 2004.

[34] P. Romanov and D. Tarpley, "Estimation of snow depth over open prairie environments using GOES imager observations," *Hydrol. Process*, vol. 18, no. 6, pp. 1073–1087, Apr. 2004.

[35] P. Romanov and D. Tarpley, "Automated monitoring of snow cover over South America using GOES Imager data," *Int. J. Remote Sens.*, vol. 24, no. 5, pp. 1119–1125, Mar. 2003.

[36] T. Lillesand, D. Meisner, A. Downs, and R. Deuell, "Use of goes and Tiros Noaa satellite data for snow-cover mapping," *Photogramm. Eng. Remote Sens.*, vol. 48, no. 2, pp. 251–259, Feb. 1982.

[37] R. LaPlante, "Real-time monitoring of lake effect snow using the WSR-88D and multispectral GOES-8 satellite imagery," in *Proc. Ocean Community Conf., Celebrating Int. Year Ocean*, 1998, pp. 40–44.

[38] A. Kennedy and C. Jones, "GOES-16 observations of blowing snow in horizontal convective rolls on 24 February 2019," *Mon. Weather Rev.*, vol. 148, no. 4, pp. 1737–1750, Apr. 2020.

[39] I. Goodwin, "Washington ins and outs-does snow goes to Chicago - Marquet and Kerber leave Dod," *Phys. Today*, vol. 41, no. 2, pp. 52–52, Feb. 1988.

[40] S. Surer, J. Parajka, and Z. Akyurek, "Validation of the operational MSG-SEVIRI snow cover product over Austria," *Hydrol. Earth Syst. Sci.*, vol. 18, no. 2, pp. 763–774, Feb. 2014.

[41] S. Terzago, R. Cremonini, C. Cassardo, and S. Fratianni, "Analysis of snow precipitation during the period 2000-09 and evaluation of a MSG/SEVIRI snow cover algorithm in Sw Italian Alps," *Geografia Fisica e Dinamica Quaternaria*, vol. 35, no. 1, pp. 91–99, May 2012.

[42] S. Surer, O. Gokdemir, O. Beser, Z. Akyurek, A. U. Sorman, and A. G. Erturk, "Real time snow recognition from MSG satellite for mountainous areas," in *Proc. Remote Sens. Changing Europe*, Jan. 2009, pp. 86–93.

[43] P. Boi, "Snow cover retrieval over Italy and alpine regions using MSG data for climatologic purposes," *Meteorol. Appl.*, vol. 17, no. 3, pp. 313–320, Sep. 2010.

[44] S. Li, H. Yan, and C. Liu, "Study of snow detection using FY-2C satellite data," *J. Remote Sens.*, vol. 11, no. 3, pp. 406–413, Feb. 2007.

[45] Y. Zhou, H. Jiang, X. Yang, and E. Geng, "NDSI products system based on hadoop platform," in *Proc. Int. Conf. Intell. Earth Observ. Appl.*, 2015, pp. 197–204.

[46] H. Zhang et al., "Ground-based evaluation of MODIS snow cover product V6 across China: Implications for the selection of NDSI threshold," *Sci. Total Environ.*, vol. 651, pp. 2712–2726, Feb. 2019.

[47] V. Salomonson and I. Appel, "Development of the Aqua MODIS NDSI fractional snow cover algorithm and validation results," *IEEE Trans. Geosci. Remote Sens.*, vol. 44, no. 7, pp. 1747–1756, Jul. 2006.

[48] J. Centeno, E. Mitishita, and R. Kishi, "Assessing snow extent variations of Illimani Mountain with Landsat NDSI," in *Proc. IEEE Int. Geosci. Remote Sens. Symp.*, 2017, pp. 616–619.

[49] S. Ali, M. Cheema, M. Waqas, M. Waseem, U. Awan, and T. Khaliq, "Changes in snow cover dynamics over the Indus Basin: Evidences from 2008 to 2018 MODIS NDSI trends analysis," *Remote Sens.*, vol. 12, no. 17, Sep. 2020, Art. no. 2782.

[50] J. Shi and J. Dozier, "Mapping seasonal snow with SIR-C/X-SAR in mountainous areas," *Remote Sens. Environ.*, vol. 59, no. 2, pp. 294–307, Feb. 1997.

[51] T. Nagler and H. Rott, "Retrieval of wet snow by means of multitemporal SAR data," *IEEE Trans. Geosci. Remote Sens.*, vol. 38, no. 2, pp. 754–765, Mar. 2000.

[52] Q. Zhang, Y. Yu, W. Zhang, T. Luo, and X. Wang, "Cloud detection from FY-4A's geostationary interferometric infrared sounder using machine learning approaches," *Remote Sens.*, vol. 11, no. 24, Dec. 2019, Art. no. 3035.

[53] T. Wang, J. Luo, J. Liang, B. Wang, W. Tian, and X. Chen, "Comparisons of AGRI/FY-4A cloud fraction and cloud top pressure with MODIS/Terra measurements over East Asia," *J Meteorol. Res.*, vol. 33, no. 4, pp. 705–719, Aug. 2019.

[54] Z. Tan, S. Ma, D. Han, D. Gao, and W. Yan, "Estimation of cloud base height for FY-4A satellite based on random forest algorithm," *J. Infrared Millim. Wave*, vol. 38, no. 3, pp. 381–388, Jun. 2019.

[55] B. Chen, Q. Wu, X. Feng, Q. Guo, and C. Wei, "On-orbit test to FY-4A AGRI and generating RBG image," *J. Infrared Millim. THz Waves*, vol. 37, no. 4, pp. 411–415, Aug. 2018.

[56] P. Li and D. Mi, "Distribution of snow cover in China," *J. Glaciol. Geocryol.*, vol. 5, no. 4, pp. 9–18, Dec. 1983.

[57] Z. Zhong, X. Li, X. Xu, X. Liu, and Z. He, "Analysis of temporal and spatial changes of snow cover in China from 1992 to 2010," *Chin. Sci. Bull.*, vol. 63, no. 25, pp. 2641–2654, Dec. 2018.

[58] X. Li, S. Liang, K. Zhao, J. Wang, T. Che, and Z. Li, "Snow cover classification based on climate variables and its distribution characteristics in China," *J. Glaciol. Geocryol.*, vol. 42, no. 1, pp. 62–71, Jun. 2020.

[59] J. Wang et al., "Investigation on snow characteristics and their distribution in China," *Adv. Earth Sci.*, vol. 33, no. 1, pp. 12–26, Jan. 2018.

[60] Y. Zhang, H. Cao, and X. Kan, "Snow cover recognition for Xinjiang based on fusion of FY-4A/AGRI spatial and temporal characteristics," *Remote Sens. Technol. Appl.*, vol. 35, no. 6, pp. 1337–1347, Dec. 2020.

[61] X. Huang, T. Liang, and X. Zhang, "Validation of MODIS snow cover products using Landsat and ground measurements during the 2001–2005 snow seasons over Northern Xinjiang, China," *Int. J. Remote Sens.*, vol. 32, no. 1/2, pp. 133–152, Feb. 2011.

[62] M. I. Gladkova, G. Bonev, P. Romanov, and F. Shahriar, "Increasing the accuracy of MODIS/Aqua snow product using quantitative image restoration technique," *IEEE Trans. Geosci. Remote Sens.*, vol. 9, no. 4, pp. 740–743, Jul. 2012.

[63] B. Ramsay, "The interactive multisensor snow and ice mapping system," *Hydrol. Process*, vol. 12, no. 10, pp. 1537–1546, Dec. 1998.

[64] S. Helfrich, D. McNamara, B. Ramsay, T. Baldwin, and T. Kasheta, "Enhancements to, and forthcoming developments in the interactive multisensor snow and Ice Mapping System (IMS)," *Hydrol. Process*, vol. 21, no. 12, pp. 1576–1586, May. 2007.

[65] A. Friedl et al., "MODIS collection 5 global land cover: Algorithm refinements and characterization of new datasets," *Remote Sens. Environ.*, vol. 114, no. 1, pp. 168–182, Aug. 2010.

[66] L. Roujean, M. Leroy, and P. Deschamps, "A bidirectional reflectance model of the Earth's surface for the correction of remote sensing data," *J. Geophys. Res. Atmos.*, vol. 97, no. 18, pp. 20455–20468, Dec. 1992.

[67] H. Qiao and Y. Zhang, "FY-3C and FY-4A satellite data were combined to study the variation of snow cover area: A case study of Qilian Mountains," *Remote Sens. Technol.*, vol. 35, no. 6, pp. 1320–1328, Dec. 2020.

[68] G. Yang, H. Xie, T. Yao, and C. Xue, "Integrated assessment on multitemporal and multi-sensor combinations for reducing cloud obscuration of MODIS snow cover products of the Pacific Northwest USA," *Remote Sens. Environ.*, vol. 114, no. 8, pp. 1662–1675, Feb. 2010.

[69] Y. Gao, H. Xie, N. Lu, T. Yao, and T. Liang, "Toward advanced daily cloud-free snow cover and snow water equivalent products from Terra–Aqua MODIS and Aqua AMSR-E measurements," *J. Hydrol.*, vol. 385, no. 1–4, pp. 23–35, Jan. 2010.

[70] C. Liu, Z. Li, P. Zhang, J. Zeng, and Z. Zheng, "An assessment and error analysis of MOD10A1 snow product using Landsat and ground observations over China during 2000-2016," *IEEE J. Sel. Topics Appl. Earth Observ. Remote Sens.*, vol. 13, pp. 1467–1478, 2020.

[71] K. Rittger, T. Painter, and J. Dozier, "Assessment of methods for mapping snow cover from MODIS," *Adv. Water Resour.*, vol. 51, pp. 367–380, Mar. 2013.

[72] H. Zhang et al., "Ground-based evaluation of MODIS snow cover product V6 across China: Implications for the selection of NDSI threshold," *Sci. Total Environ.*, vol. 651, no. PT. 2, pp. 2712–2726, Oct. 2018.

[73] X. Liu, X. Jin, and C. Ke, "Accuracy evaluation of the IMS snow and ice products in stable snow covers regions in China," *J. Glaciol. Geocryol.*, vol. 36, no. 3, pp. 500–507, Jun. 2014.

[74] H. Liang, "Research on the mapping algorithm of MODIS snow area proportion on the Tibetan Plateau," M.S. thesis, Dept. Grassol., Lanzhou Univ., Gansu, China, 2019.

[75] X. Y. Wang, C. Y. Wu, H. J. Wang, A. Gonsamo, and Z. J. Liu, "No evidence of widespread decline of snow cover on the Tibetan Plateau over 2000-2015," *Sci. Rep.*, vol. 7, no. 1, pp. 14645–14651, Nov. 2017.

[76] Q. You, T. Wu, L. Shen, N. Pepin, and A. Aghakouchak, "Review of snow cover variation over the Tibetan Plateau and its influence on the broad climate system," *Earth-Sci. Rev.*, vol. 201, Feb. 2020, Art. no. 1030.

[77] C. Han, "Improvement and application of snow detection algorithm using the new generation of geostationary meteorological satellite," M.S. thesis, Dept., Meteorol., Nanjing Univ. Informat. & Technol., Jiangsu, China, 2018.

[78] A. Muhuri, S. Gascoin, L. Menzel, T. Kostadinov, and J. Moreno, "Performance assessment of optical satellite based operational snow cover monitoring algorithms in forested landscapes," *IEEE J. Sel. Topics Appl. Earth Observ. Remote Sens.*, vol. 14, pp. 7159–7178, 2021.

[79] X. Wang, J. Wang, H. Li, and X. Hao, "Combination of NDSI and NDFSI for snow cover mapping in a mountainous and forested region," *J. Remote Sens.*, vol. 21, no. 2, pp. 310–317, Mar. 2017.

**Ping Zhang** received the Ph.D. degree in communication and information system from Institute of Electronics, Chinese Academy of Sciences, Beijing, China, in 2009.

Currently, she is an Associate Professor with the Key Laboratory of Digital Earth Science, Aerospace Information Research Institute, Chinese Academy of Sciences. She has authored and coauthored more than 20 articles and three book chapters.

Her current research activities include concentrated in remote sensing data processing, signal processing, and calibration of SAR.

**Zhen Li** (Member, IEEE) received the B.S. degree in photogrammetry and remote sensing from Wuhan University, Wuhan, China, in 1988, and the Ph.D. degree in natural geography from the Cold and Arid Regions Environmental and Engineering Research Institute, Chinese Academy of Sciences, Lanzhou, China, in 1998.

He is currently a Professor with the Key Laboratory of Digital Earth Science, Aerospace Information Research Institute, Chinese Academy of Sciences, Beijing, China. He has authored more than 100 journal papers and has authored and coauthored 4 books in collaboration with others. His current research interests include microwave remote sensing, cryosphere environment, and disaster remote sensing.

**Haiwei Qiao** received the B.S. degree in geographical information science from Northwest Normal University, Lanzhou, China, in 2020. He is currently working toward the Ph.D. degree in cartography and geography information system with the Key Laboratory of Digital Earth Science, Aerospace Information Research Institute, Chinese Academy of Sciences, Beijing, China.

His current research interests include InSAR technology and application, TomoSAR technology and application, and snow remote sensing.

**Chang Liu** received the B.S. degree in remote sensing science and technology from Shandong University of Science and Technology, Shandong, China, in 2017. She is currently working toward the Ph.D. degree in cartography and geography information system with the Key Laboratory of Digital Earth Science, Aerospace Information Research Institute, Chinese Academy of Sciences, Beijing, China.

Her current research interests include assessment and application of snow products, and microwave remote sensing of snow parameters.